



Role of magnetic forces in pulse electrochemical deposition of Ni–nanoAl₂O₃ composites

Subramanian Mohan^{a,*}, Gengan Saravanan^a, Andreas Bund^b

^a Electroplating and Metal Finishing Technology Division, CSIR – Central Electrochemical Research Institute, Karaikudi – 630006, India

^b Institute of Physical Chemistry and Electrochemistry, Dresden University of Technology, D-01062, Germany

ARTICLE INFO

Article history:

Received 17 September 2011

Received in revised form 2 November 2011

Accepted 28 December 2011

Available online 8 January 2012

Keywords:

Nickel

Metal matrix composites

EIS

XRD

Alkaline corrosion

Electrodeposited films

ABSTRACT

Pure and composite nickel deposits containing nano-Al₂O₃ particle (50 nm) were produced under direct current (DCED) and pulsed current electrodeposition (PCED) conditions in the presence of magnetic field (MF). The influence of MF on the co-deposition of Al₂O₃ particles, texture coefficient of Ni and Al₂O₃, crystallite size, thickness, current efficiency and hardness of the deposits were investigated systematically. PCED regime exhibited higher incorporation nano-Al₂O₃ percentage than those obtained under DCED condition. The electrochemical impedance spectroscopy results show several order higher R_{ct} and lower i_{corr} for PCED Ni–Al₂O₃ in the presence of magnetic field (MF) than that of DCED Ni–Al₂O₃ composites.

© 2012 Elsevier Ltd. All rights reserved.

1. Introduction

Recent years, metal matrix nanocomposite (MMNCs) coatings have got much attention for its excellent mechanical properties such as wear resistance, mechanical [1], corrosion resistance and lubrication [2,3]. However, one of the challenges is dispersal of the particles in a common electrolyte can be problematic. In most cases agglomeration and sedimentation of the particles occurs which makes successful co-deposition difficult. A diversity of nanosized particles, such as SiC [4], SiO₂ [5], Al₂O₃ [6,7], ZrO₂ [8] have been successfully co-deposited with several metals. It is well known that the application of magnetic field can enhance mass transport in electrochemical reactions. This effect is called magnetic hydrodynamic effect (MHE) [2] and is caused by magnetic forces which induce convective movement in the electrolyte. The best investigated magnetic force in electrochemical reactions is the Lorentz force density, which induces fluid motion and thus can enhance the mass transport [9]. Eq. (1)

$$\mathbf{f}_L = \mathbf{j} \times \mathbf{B} \quad (1)$$

Furthermore, the magnetic nanoparticles will move in the electrolyte towards regions with higher magnetic flux density due to magnetophoretic force (Eq. (2)) [10].

$$\mathbf{f}_{mp} = \frac{\Delta\chi}{\mu_0} (\mathbf{B} \cdot \nabla) \mathbf{B} \quad (2)$$

where \mathbf{j} is the current density, \mathbf{B} is the magnetic flux density (bold faces symbolize vector quantities) χ is the susceptibility of the particles and μ_0 is the magnetic permeability of the free space. Notice that \mathbf{f}_L acts on fluid elements whereas \mathbf{f}_{mp} acts on the particles themselves. The circulation velocity was proportional to the intensity of magnetic flux density. The circulation velocity on the electrode was about 10 times higher than the average circulation velocity. It is considered that circulation produced by Lorentz force was effective, compared with mechanical or air mixing, in ensuring that the incorporation of particles. Magnetic field, as a controllable method, has been attempted to be adopted in the electrochemical process. Hu and Chan [11] discovered that the polarization curves and the SiC content in nickel matrix as well as the corrosion resistance of composite coatings could be influenced by magnetic field. Thanks to superconductive technology for providing magnetic flux density (MFD) more than 1 T for the past two decades. Ispas et al. [12] conducted frequency-dependence of linear and second harmonic AC response differential measurements disclosed that the kinetics of the adsorption process occurs during Ni–Fe alloy deposition influenced by the additional mass-transport brought about by magnetically driven convection. Zhong et al. [13]

* Corresponding author. Tel.: +91 4565 227551; fax: +91 4565 227713.
E-mail addresses: mohan40159@cecri.res.in, sanjnamohan@yahoo.com (S. Mohan).

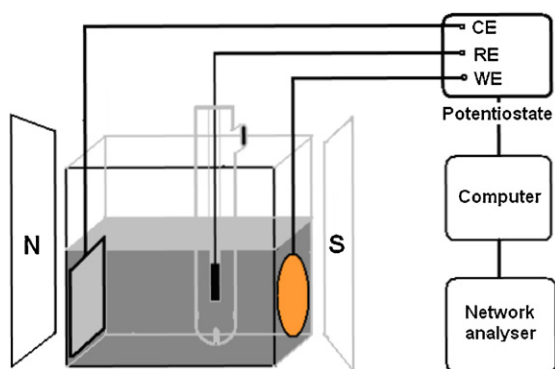


Fig. 1. Schematic diagram of the experimental setup for the Ni–Al₂O₃ composite deposition in perpendicular magnetic field (\mathbf{B} field), N north pole, S south pole of magnet, CE counter electrode, WE working electrode and RE reference electrode.

reported that magnetic field improved the particle content incorporated into nickel matrix increased about 8 wt% of particle content under 0.7 T MF. MHD not only enhanced mass transport process but also improve the discharge reaction. Thiemig et al. [14] reported recently both pulse and pulse reverse electrodeposition controlling both particle content and properties of MMNCs. This is our first report explaining current efficiency, hardness, structural composition, anticorrosive properties of Ni/Al₂O₃ under PCED in the presence of MHD force. The structures of Ni–Al₂O₃ composition were analyzed by XRD, SEM and EDS respectively.

2. Experimental

A typical three-electrode cell was used for electrochemical experiments. The effective area of the working electrode (WE made from Cu) was around 0.38 cm², counter electrode (CE) was a Pt foil of approximately 3 cm × 7 cm area and 0.2 mm thickness, placed in parallel to the WE. The distance between the WE and CE was approximately 2 cm. The WE was fixed vertical in the cell, parallel to the gravity. Saturated calomel electrode (SCE) used as reference electrode, nickel and Ni–Al₂O₃ deposition were carried out from 240 g/L NiSO₄ and 45 g/L NiCl₂ (pH = 4 ± 0.3) in highly purified water at 2 A dm⁻². A detailed description of the experimental setup of the magneto-electrodeposition setup is shown in Fig. 1.

The magnetic field (with flux up to 0.5 T) was superimposed from a water-cooled electromagnet (VEB Polytechnik, Phylatex, Chemnitz, Germany). The structural morphology of the deposited Ni and Ni–Al₂O₃ composites was investigated using a FEI Quanta 600 and Zeiss DSM 982 scanning electron microscope. Furthermore, EDX analyses were performed on the surface for the amount of Al₂O₃ particle incorporation. The accuracy of EDX analysis was approximately ±0.5 vol%. An average was taken from three randomly chosen points. X-ray diffractogram was recorded with a scan step size of 0.0171° and step time is 10.3366 s for 2 θ ranging from 10 to 100° (PANalytical model X'pert PRO) X-ray diffractometer using Cu K α , λ = 0.1540 nm. The size of the nickel and Al₂O₃ crystallites were determined from the broadening of the peaks reflections according to the Debye–Scherrer equation [15]. The surface morphology and the distribution of particles within the metal matrix were investigated using a FEI Quanta 600 and Zeiss DSM 982 scanning electron microscope. Furthermore, EDX analysis was (655 μ m²) performed with accuracy ±0.5 vol% average was taken from three randomly chosen points. Everyone (MH-series) microhardness tester with Vickers indent was used to determine hardness of Ni–Al₂O₃ composites.

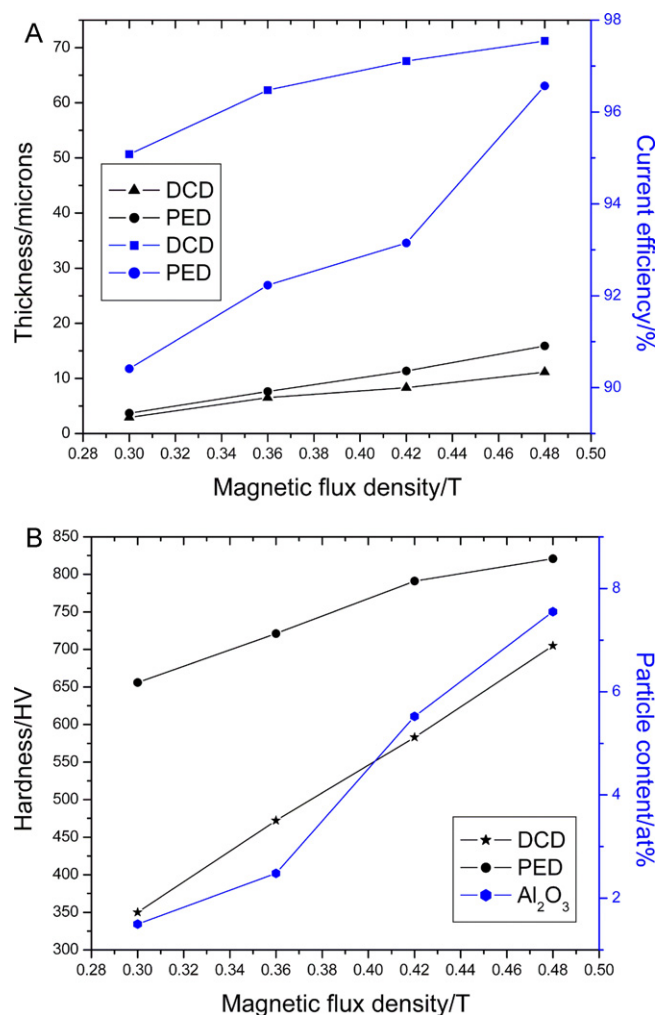


Fig. 2. (A) Effect of magnetic field (a) direct current (DCED), (b) pulse current electrodeposition on thickness and current efficiency of Ni–Al₂O₃ nanocomposite. (B) Effect of magnetic field (a) direct current (DCED) and (b) pulse current electrodeposition on hardness and Al₂O₃ particle content.

3. Results and discussion

3.1. DCED VS. PCED

PCED significantly raises the limiting current density (I_L) by replenishing metal ions in the diffusion layer only during T_{OFF} . In the conventional DCED there is only one parameter, namely current density (I), which can be varied. But in PCED, we have three independent variables, viz., (i) ON-time (T_{ON}), (ii) OFF-time (T_{OFF}) and (iii) peak current density (I_P). The pulse T_{ON} must be less than the transition time (τ), time required for the interfacial concentration to reach zero and much longer than the charging time (t_c) in microseconds. The value of pulse I_L might for exceed DCED limiting current density (I_G). In PCED, high I_P enhances the adatoms population and nucleation rate during T_{ON} . PCED can control the electro crystallization mechanism and controls the physical and mechanical properties of the electrodeposited metal [16].

3.2. Effect of magnetic field on thickness and current efficiency under DCED and PCED

From Fig. 2A it is noted that the electrolytic currents are enhanced by applying perpendicular magnetic field during electrodepositing Ni–Al₂O₃ films. It is well known that the MHD

convection induced by Lorentz force could reduce the thickness of diffusion layer and concentration polarization, thus enhance the mass transport process [17,18]. In other words, MHD effect leads to a convective movement of Ni^{2+} , nano-alumina particles, and other involved reagents to the electrode surface, and for the electrochemical systems limited by the mass transport which induced an increase of the electrolytic current. Bund et al. [19] thought that the enhanced phenomenon was ascribed to interplay of natural convection and forced convection induced by Lorentz force. As $\alpha\text{-Al}_2\text{O}_3$ particle was surrounded by a thin layer of adsorbed Ni^{2+} and H_3O^+ ions after being immersed in Watts electrolyte, the more adsorption of nano-particles, ions reached the cathode surface and eventually increases the reduction current.

Fig. 2A shows that the thickness of composite coatings was increased with particle content increase, which is in agreement with the results by Pushpavanam and Shenoi [20]. It means that the magnetic field improved the deposition rate of composite coatings. Bund and co-workers [21] got different results. They hypothesized that the current efficiency of Ni electrodeposition was 100%, thus, the current efficiency increases with increase of particle content is increased. It is well known that the co-deposition phenomenon always goes with the reduction reaction of H^+ as mentioned above, $\alpha\text{-Al}_2\text{O}_3$ particle were surrounded by a thin layer of adsorbed Ni^{2+} and H_3O^+ ions. After the particles were introduced in Watts's electrolyte, more Al_2O_3 particles were adsorbed on the cathode surface, more H^+ were reduced. Experimental results showed that the MHD convection increased the mass transport of protons, which were involved as a secondary reaction in the electrochemical mechanism in nickel electrodeposits [22] and in iron electrodeposition [20].

3.3. Effect of magnetic field on hardness

An increase in the hardness of a material is always associated with an increase in its resistance against ductile deformation and thus against the generation and sliding of dislocations (Fig. 2B). For the nano-MMCs produced in this study, have two possible hardening and strengthening mechanisms: the hardening by grain refinement [23] of the matrix and the dispersion hardening by particles [24]. The particles act as obstacles to dislocation movements and cause the hardening of the material. The hardening by grain refinement is based on the increasing number of grain boundaries and triple junctions due to the decreasing grain size. In this case, the grain boundaries and triple junctions act as obstacles to the dislocation movement. There are several mechanisms which describe the interactions of the dislocations with the dispersed particles in the metal matrix. The hardening by particles due to particle shearing takes place only for coherent particles with a similar lattice structure as that of the host metal [25]. If a dislocation strikes a particle, the dislocation enters into the particle, passes through and shears it on a slipping plane. This causes new additional surface area which requires interfacial energy and is responsible for the strengthening of the material [26].

3.4. XRD analysis

Fig. 3 gives X-ray diffraction pattern of Ni– Al_2O_3 electrodeposition in the presence of magnetic field under DCED and PCED techniques. The magnetic field has little influence on (220) and (111) plane, for both techniques (220) was the preferred orientation. In PCED we found new crystallographic phase of Al_2O_3 nanoparticles, so XRD data is also provides another evidences of increasing incorporation of Al_2O_3 particles. The crystallite sizes of Ni and Ni– Al_2O_3 composites coatings were calculated from Debye–Scherrer equation $D = 0.94\lambda / \beta \cos \theta$ [15]. Where D is the grain size, β is the full width at half maximum (FWHM) of the diffraction peak, λ is the wavelength of the incident X-ray (1.54 Å),

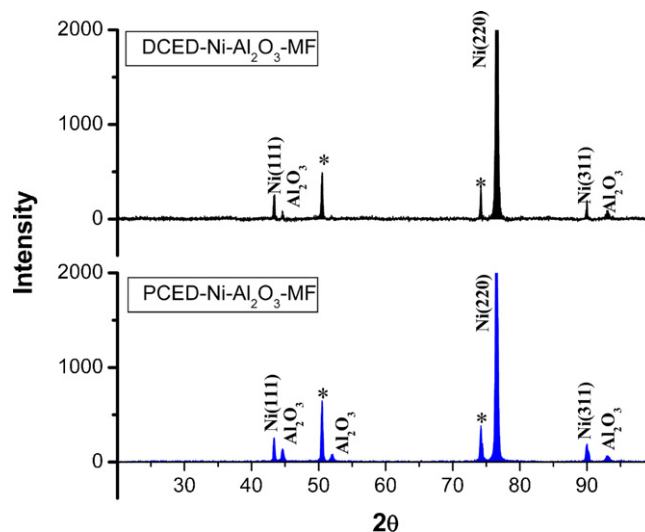


Fig. 3. X-ray diffraction pattern of Ni– Al_2O_3 electrodeposited nanocomposite obtained in both DCED and PCED techniques.

and θ is the diffraction angle. The average crystallite sizes were calculated and the values vary from 42 to 48 nm and 23 to 27 nm for Ni and Al_2O_3 nanoparticles respectively.

3.5. Surface morphology, microstructural and microchemical characterization

SEM micrograph revealed that the Ni grain structure of the truncated pyramidal type (Fig. 4A and D), where a cluster of fine grains surrounds relatively large grains of DCED. The grains size and shape of the Ni films were significantly reduced and altered due to current interrupted PCED techniques. In the case of PCED the number of atoms deposited during cathodic cycle is defined by t_{on} and i_p sorption process occurring during pulse pause which may influence nucleation and growth process [27]. Ni– Al_2O_3 composite size and shape of the grains were significantly altered due to direct, pulsed current condition and incorporation of Al_2O_3 nanoparticles (Fig. 4B and E). In the case of Ni– Al_2O_3 composites the agglomerations of Al_2O_3 particles appear as bright spots in the dark nickel matrix under DCED. Condition, validated by energy dispersive X-ray spectroscopy (Fig. 2B). The nickel growth is affected by several interfacial inhibitors such as H_2 , H_{ads} , $\text{Ni}(\text{OH})_2$ [28]. It is assumed that PCED conditions as well as particle incorporation perturb the nickel growth and induce an increase the number of nucleation sites resulting in a refined grain structure [29] thereby the perturbation of the crystal growth results from a change in the adsorption–desorption phenomena at the Ni/electrolyte interface which is probably caused by a local pH increase induced by an adsorption of H^+ to be dispersed particles [30]. The application of magnetic field improved the particle content incorporated into Ni matrix in the case of PCED than DCED techniques. This is due to combined effect of MHD condition due to eddy vortices and reduces the thickness of the diffusion layer as a result of increasing concentration gradient (Fig. 4C and F).

The particle content in composite coatings (Fig. 2B) clearly shows that with increasing of magnetic flux density, the content of particles in composite coatings increases. When imposing of a high magnetic field in the process of electrodeposition, an eddy motion could be induced to agitate the electrolyte. Thus, the nano- Al_2O_3 particles should be transported to the cathode surface for the co-deposition. When the magnetic field density increases, the fluid flow is capable of transporting Al_2O_3 particles to the substrate and

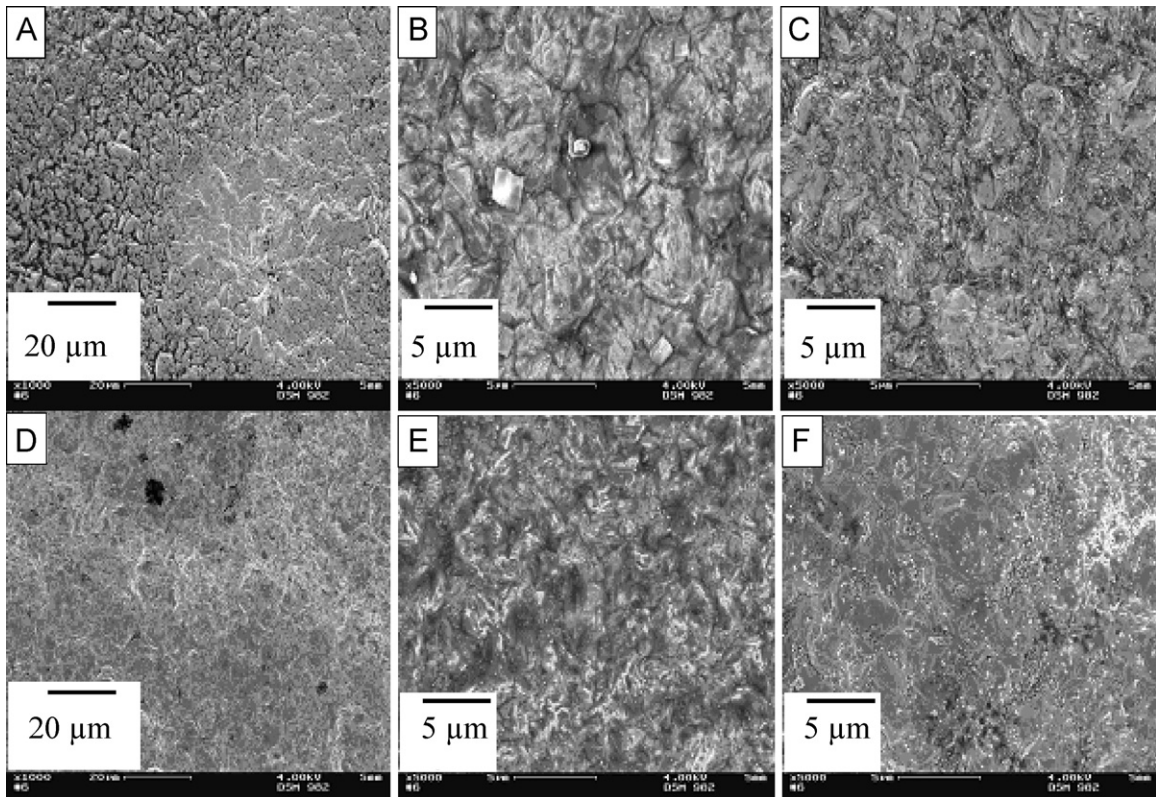


Fig. 4. Scanning electron microscopy of coatings obtained with and without magnetic field at 2 A dm^{-2} current density (1: 0 T DCED pure Ni; 2: 0 T DCED pure Ni– Al_2O_3 ; 3: 0.4 T DCED Ni– Al_2O_3 ; 4: 0 T PCED pure Ni; 5: 0 T PCED pure Ni– Al_2O_3 ; 6: 0.4 T PCED Ni– Al_2O_3).

the co-deposition behavior of nano- Al_2O_3 particles is apparently controlled by particles transfer.

3.6. Electrochemical impedance spectroscopy

In order to investigate the effect of MF on the composite process, the EIS of the process were examined. Fig. 5 gives the Nyquist plot of EIS curves with various MF strengths. In Nyquist diagram,

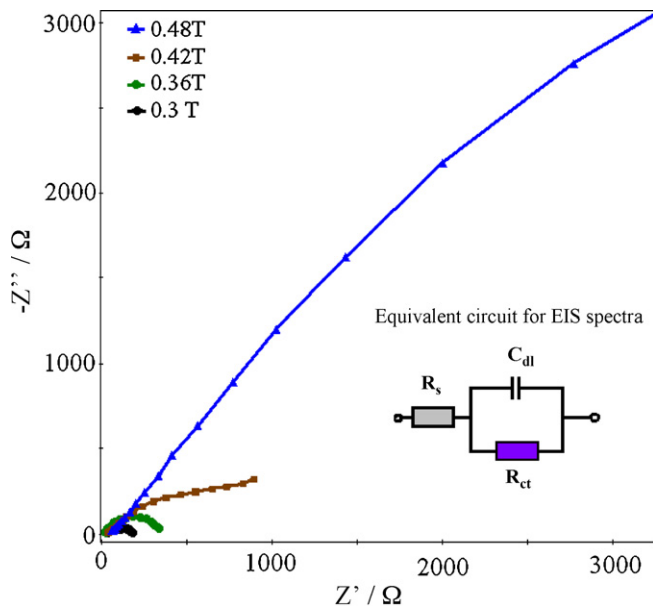


Fig. 5. Electrochemical impedance spectroscopy of electrodeposited Ni– Al_2O_3 system at different magnetic field.

the composites coatings revealed one semicircle which indicates single electron transfer process. For Ni– Al_2O_3 composite coatings the diameter of semicircle on Nyquist plots increases with increasing magnetic field. Such behavior indicates that the charge transfer resistance is changed in the presence of magnetic field. The equivalent circuit (insert in Fig. 5) is used to fit the corrosion resistance parameters. R_{ct} and C_{dl} represent the charge-transfer resistance and double-layer capacitance, respectively. The fitted impedance spectra are in good agreement with the impedance spectra recorded during the measurements, as shown in Fig. 5. The calculated values of circuit elements are listed in Table 1. The charge transfer resistance increased from $183 \Omega \text{ cm}^2$ in 0.3 T to $28,180 \Omega \text{ cm}^2$ in 0.48 T magnetic fields. Increase of R_{ct} with increasing of MF is due to enhancement of incorporation of $\text{SiC}/\text{Al}_2\text{O}_3$ which diminishes the exposed metallic area [31,32]. Increased amount of Al_2O_3 is considered to be attributing to the improvement of mass transport process but also improved the discharge reaction. The MF enhanced the limiting current density in unstirred solution enhancement stronger (5–10%) than that in stirred solution (2–5%) [33]. The ions moving with velocity v in the electrolytic solution will be subject to the effect of Lorentz force ($qv \times B$) shown in Fig. 6A and B. When nanoparticles were added into electrolytic solution, the electrolytic current distorted in the vicinity of a particle, because the nanoparticles are inert and non-conducting ones as illustrated in Fig. 6B.

Table 1

Corrosion parameters obtained from polarization studies and impedance measurements by Nyquist plots in 3.5% w/v NaCl solution.

Magnetic field	i_{corr} (A cm^2)	R_{ct} ($\Omega \text{ cm}^2$)	CR (mppy)
0.3 T	8.8×10^{-5}	183	2.4958
0.36 T	3.3×10^{-5}	365	0.9470
0.4 T	1.3×10^{-5}	1276	0.3780
0.46 T	1.2×10^{-6}	28,180	0.0340

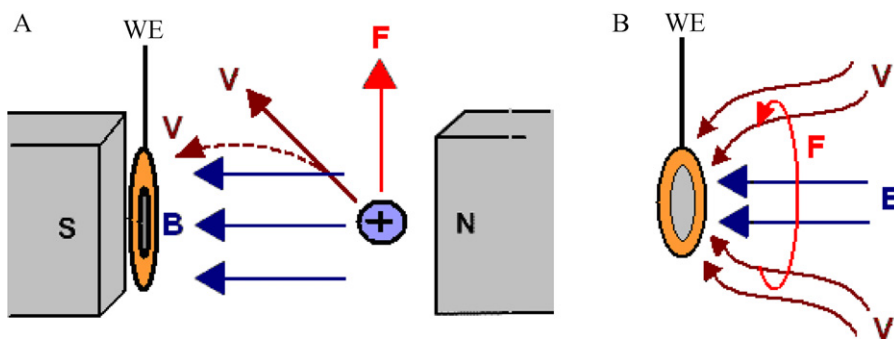


Fig. 6. (A and B) Schematic sketch of the experimental setup of the electrodeposition in a perpendicular (Z-direction) magnetic field. WE working electrode. The vectors V , B and F indicate the actual direction of the current density, the magnetic flux density, and the Lorentz force, respectively.

In this case, the electrolytic current had an orthogonal component to the magnetic field [34] direction as shown in Fig. 7. CR is corrosion rate whose value is decreased when increasing MF strength. When a magnetic field is applied perpendicular to the electrode, a localized convection introduces a hydrodynamic drag out, which acts on the hydrogen bubble (obstacle in the flow). The contact angle increases (weaker adhesion), due to the drag force action, H_2 bubbles could be removed from the electrode surface. As a consequence, enhanced desorption of H_2 is observed [34]. Therefore, micro holes free smooth Ni– Al_2O_3 nano composites obtained. Therefore, the Lorentz force is induced by the interaction of an imposed magnetic field and a distorted electrolytic current. In the electroplating electrolyte, the MHD flow generated by the Lorentz force proceeded on the electrode surface, and many minute vortices emerged above the surface [35]. In total, the motion of numerous eddy vortices near the cathode surface will lead to the convection of electrolytic solution. This is the stirring effect of MHD convection, which can affect the morphology of the deposits. Through the MHD convection, the electrolytic solution will be stirred and the dispersing power will be enhanced. Thus, the MHD convection reduces the thickness of the diffusion layer and consequently, results in an increasing concentration gradient, which should have an effect on the grain size [36] and morphological variations [37]. Hinds et al. [18] also proposed that the effect of the magnetic field is to induce convection in the solution and it is equivalent to rotating the electrode or stirring the solution. When a MF is applied perpendicular to the electrode, a localized convection introduces a hydrodynamic drag force [38], which acts on the hydrogen bubble. The contact angle increases (weaker adhesion), due to the drag force action, H_2

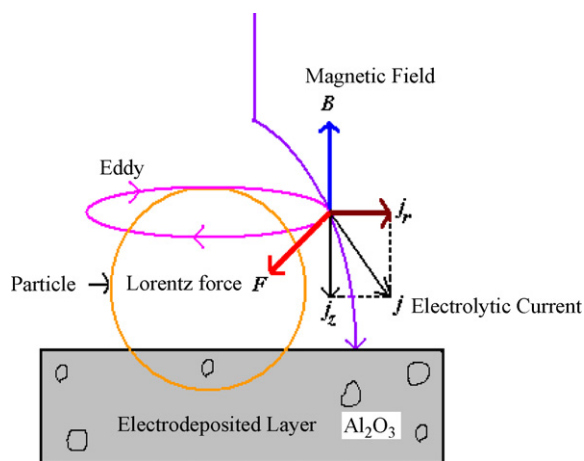


Fig. 7. Schematic view showing a principle to generate eddy motion in the vicinity of a particle due to the interaction of a magnetic field and a distorted electrolytic current.

bubbles could be removed from the electrode surface. As a consequence, enhanced desorption of H_2 take place. This situation can be derived from the surface morphology of Ni– Al_2O_3 layer deposited under the perpendicular MF of 0.48 T, where no holes remained after H_2 bubbles were formed.

Compared to DC electrodeposition, pulse electrodeposition can yield nanocrystalline coatings with improved surface appearance and properties such as smoothness, refined grains and enhanced corrosion resistance [39,40]. Particle incorporation showed a tendency to increase with the cycle as well as increasing the pulse frequency. Decreasing the duty cycle as well as increasing the pulse frequency corresponds to a longer relaxation (T_{OFF}) time.

4. Conclusions

The electrodeposition of Ni– Al_2O_3 composites using a Watts bath has been carried out in a high magnetic field and the wear resistance of electrodeposited Ni– Al_2O_3 composites has been investigated.

- The following are the salient conclusions of the present study: it is feasible to prepare Ni– Al_2O_3 nanocomposite coating in a high magnetic field instead of mechanical agitation.
- In PCED the amounts of nano- Al_2O_3 particles in the composite coating increase with increasing magnetic flux density, and reach a maximum value and hence hardness of deposits enhanced.
- Eddy motion generates around each particle due to the interaction of an imposed magnetic field and an electrolytic current distorted by the existence of non-conducting particles. R_{ct} value of PCED Ni– Al_2O_3 in the presence of MF is several orders higher than that of DCED Ni– Al_2O_3 composites.

Acknowledgements

The authors gratefully acknowledge the DAAD for fellowship under CSIR-DAAD exchange of scientists' programme 2010.

References

- [1] Y.-J. Xue, D. Zhu, F. Zhao, J. Mater. Sci. 39 (2004) 4063.
- [2] J.L. Stojak, J. Fransaer, J.B. Talbot, in: R.C. Alkire, D.M. Kolb (Eds.), Adv. Electrochem. Sci. Eng., Wiley-VCH Verlag, Weinheim, 2002.
- [3] V. Medelienė, V. Stankevič, G. Bikulcius, Surf. Coat. Technol. 168 (2003) 161.
- [4] M. Kaisheva, J. Fransaer, J. Electrochem. Soc. 151 (2004) C89.
- [5] V. Terzieva, J. Fransaer, J.-P. Celis, J. Electrochem. Soc. 147 (2000) 198.
- [6] G. Vidrich, J.-F. Castagnet, H. Ferkel, J. Electrochem. Soc. 152 (2005) C294.
- [7] A. Bund, D. Thiemi, Surf. Coat. Technol. 201 (2007) 7092.
- [8] F. Hou, W. Wang, H. Guo, Appl. Surf. Sci. 252 (2006) 3812.
- [9] R.A. Tacken, L.J.J. Janssen, J. Appl. Electrochem. 25 (1995) 1.
- [10] G. Hinds, F.E. Spada, J.M.D. Coey, T.R.N. Mhóicháin, M.E.G. Lyons, J. Phys. Chem. B 105 (2001) 9487.
- [11] F. Hu, K.C. Chan, Appl. Surf. Sci. 233 (2004) 163.

- [12] A. Ispas, H. Matsushima, A. Bund, B. Bozzini, *J. Electroanal. Chem.* 651 (2011) 197.
- [13] C. Wang, Y.-B. Zhong, J. Wang, Z.-Q. Wang, W.-L. Ren, Z.-S. Lei, Z.-M. Ren, *J. Electroanal. Chem.* 630 (2009) 42.
- [14] D. Thiemi, A. Bund, J.B. Talbot, *Electrochim. Acta* 54 (2009) 2491.
- [15] H.P. Klug, L.E. Alexander, *X-ray Diffraction procedure*, 2nd ed., John Wiley & Sons, New York, 1974, p. 618.
- [16] M.S. Chandrasekar, M. Pushpavanam, *Electrochim. Acta* 53 (2008) 3313.
- [17] A. Bund, A. Ispas, *J. Electroanal. Chem.* 575 (2005) 221.
- [18] G. Hinds, J.M.D. Coey, M.E.G. Lyons, *Electrochem. Commun.* 3 (2001) 215.
- [19] A. Bund, S. Koehler, H.H. Kuehnlein, W. Plieth, *Electrochim. Acta* 49 (2003) 147.
- [20] M. Pushpavanam, B.A. Shenoi, *Met. Finish.* 75 (1977) 38.
- [21] R. Peipmann, J. Thomas, A. Bund, *Electrochim. Acta* 52 (2007) 5808–5814.
- [22] O. Devos, O. Aaboubi, J.P. Chopart, E. Merienne, A. Olivier, J. Amblard, *J. Electrochem. Soc.* 145 (1998) 4135.
- [23] H. Matsushima, T. Nohira, I. Mogi, Y. Ito, *Surf. Coat. Technol.* 179 (2004) 245.
- [24] G. Georgiev, I. Kamenova, V. Georgieva, et al., *Godishnik na Sofiiskiya Universitet* 159 (2006) 98.
- [25] T. Gladman, *Mater. Sci. Technol.* 115 (1999) 30.
- [26] A. Jung, H. Natter, R. Hempelmann, E. Lach, *J. Mater. Sci.* 44 (2009) 2725.
- [27] E. Budevski, G. Staikov, W.J. Lorenz, *Electrochemical Phase Formation and Growth*, VCH, Weinheim, 1996.
- [28] M. Stroumbouli, P. Gyftou, E.A. Pavlatou, N. Spyrellis, *Surf. Coat. Technol.* 195 (2–3) (2005) 325.
- [29] L. Du, B. Xu, S. Dong, H. Yang, Y. Wu, *Surf. Coat. Technol.* 192 (2005) 311.
- [30] E.A. Pavlatou, M. Stroumbouli, P. Gyftou, N. Spyrellis, *J. Appl. Electrochem.* 36 (2006) 385.
- [31] X.P. Li, Z.J. Zhao, H.L. Seet, W.M. Heng, T.B. Oh, J.Y. Lee, *Electrochem. Solid State Lett.* 7 (1) (2004) C1.
- [32] S. Legeai, M. Chatelut, O. Vittori, J.P. Chopart, O. Aaboubi, *Electrochim. Acta* 50 (2004) 51.
- [33] A. Bund, H.H. Kuehnlein, *J. Phys. Chem. B* 109 (2005) 19845.
- [34] J.A. Koza, M. Uhlemann, A. Gebert, L. Schultz, *Electrochem. Commun.* 10 (2008) 1330.
- [35] S. Yonemochi, A. Sugiyama, K. Kawamura, T. Nagoya, R. Aogaki, *J. Appl. Electrochem.* 34 (2004) 1279.
- [36] A. Krause, C. Hamann, M. Vhlemann, A. Gebert, L. Schultz, *J. Magn. Magn. Mater.* 261 (2005) 290.
- [37] M. Motoyama, Y. Fukunaka, S. Kikuchi, *Electrochim. Acta* 51 (2005) 897.
- [38] R. Philip-Chandy, R. Morgan, P.J. Scully, in: J.G. Webster (Ed.), *Measurements, Instrumentation, and Sensor Handbook*, CRC, Press, LLC, Boca Raton, 1999 (Chapter 5).
- [39] A.F. Zimmerman, D.G. Clark, K.T. Aust, U. Erb, *Mater. Lett.* 52 (2002) 85.
- [40] S. Tao, D.Y. Li, *Nanotechnology* 17 (2006) 65.